

Structure Determination of a Membrane Protein in Proteoliposomes

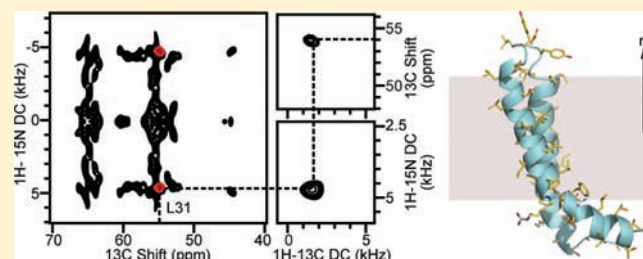
Bibhuti B. Das,[†] Henry J. Nothnagel,[†] George J. Lu,[†] Woo Sung Son,[†] Ye Tian,^{†,‡} Francesca M. Marassi,[‡] and Stanley J. Opella^{*,†}

[†]Department of Chemistry and Biochemistry, University of California, San Diego, La Jolla, California 92093-0307, United States

[‡]Sanford-Burnham Medical Research Institute, La Jolla, California 92037, United States

Supporting Information

ABSTRACT: An NMR method for determining the three-dimensional structures of membrane proteins in proteoliposomes is demonstrated by determining the structure of MerFt, the 60-residue helix–loop–helix integral membrane core of the 81-residue mercury transporter MerF. The method merges elements of oriented sample (OS) solid-state NMR and magic angle spinning (MAS) solid-state NMR techniques to measure orientation restraints relative to a single external axis (the bilayer normal) from individual residues in a uniformly ¹³C/¹⁵N labeled protein in unoriented liquid crystalline phospholipid bilayers. The method relies on the fast (>10⁵ Hz) rotational diffusion of membrane proteins in bilayers to average the static chemical shift anisotropy and heteronuclear dipole–dipole coupling powder patterns to axially symmetric powder patterns with reduced frequency spans. The frequency associated with the parallel edge of such motionally averaged powder patterns is exactly the same as that measured from the single line resonance in the spectrum of a stationary sample that is macroscopically aligned parallel to the direction of the applied magnetic field. All data are collected on unoriented samples undergoing MAS. Averaging of the homonuclear ¹³C/¹³C dipolar couplings, by MAS of the sample, enables the use of uniformly ¹³C/¹⁵N labeled proteins, which provides enhanced sensitivity through direct ¹³C detection as well as the use of multidimensional MAS solid-state NMR methods for resolving and assigning resonances. The unique feature of this method is the measurement of orientation restraints that enable the protein structure and orientation to be determined in unoriented proteoliposomes.



INTRODUCTION

About one-third of the sequences expressed from all genomes are proteins with transmembrane helices.¹ Since membrane proteins perform unique biological functions (e.g., as transporters or receptors), mutations in their sequences, as well as in the sequences of their binding partners, are linked with major human diseases,² and many membrane proteins are prime targets for drugs. This is especially true for G-protein coupled receptors, which already account for one-third of the drugs used in medicine. Until recently, the structures of only a few membrane proteins were known. However, during the past decade, substantial progress has been made through improvements in the instrumentation and experimental methods of X-ray crystallography, cryo-electron microscopy, and NMR spectroscopy, as well as in the preparation of samples for these methods.^{3,4} Because membrane proteins are not water-soluble, the initial goal of structural studies is to meet their stringent sample requirements, which typically involves the use of detergents and, in some cases, substantial modifications of their primary sequences to improve solubility or crystallization. Furthermore, some of the experimental measurements are performed at cryogenic temperatures. Each of these factors has the potential to cause distortions in the protein structure, dynamics, and activity, all of which must be sorted out with control experiments or comparisons among structures determined by multiple techniques.

Solid-state NMR spectroscopy presents the opportunity to determine the structures of membrane proteins in phospholipid bilayer membranes, under experimental conditions that are very close to physiological, without the need for major protein modifications, detergents, or extreme temperatures. The two principal techniques, oriented sample (OS) solid-state NMR⁵ and magic angle spinning (MAS) solid-state NMR,⁶ each have distinct advantages: the ability to measure accurate orientation restraints for precise structure determination (OS) and the ability to resolve and assign multiple peaks through the use of ¹⁵N/¹³C labeled unoriented samples (MAS).

OS solid-state NMR enables the measurement of orientation-dependent frequencies in the spectra of stationary uniaxially aligned samples of proteins, embedded in phospholipid bilayers, that are immobilized on the time scales (~10⁵ Hz) of the chemical shift anisotropy (CSA) and heteronuclear dipolar coupling (DC) powder patterns, except for their fast rotational diffusion around the bilayer normal. The spectra have very high resolution, with line widths that are, surprisingly, narrower than those observed for single crystals of small peptides. The principal advantage of this approach is that the orientation-dependent frequencies, which serve as the principal restraints for structure

Received: February 18, 2011

Published: January 4, 2012

determination, are derived simply and directly from the single-line spectra.⁷ These restraints simultaneously determine both the three-dimensional protein structure and orientation within the framework of the phospholipid bilayer.

This approach has enabled the structures of several membrane proteins to be determined in liquid crystalline phospholipid bilayers,^{8–13} in a few cases in combination with data from solution NMR¹⁴ or MAS solid-state NMR^{15–17} methods. The samples consist of fully hydrated protein-containing phospholipid bilayers aligned with the bilayer normal parallel or perpendicular to the direction of the applied magnetic field. Macroscopic bilayer alignment can be induced either magnetically¹⁸ or on glass surfaces.^{19,20} Magnetically aligned bilayers yield spectra with the highest resolution and are generally more stable.^{12,21,22} However, they typically require the addition of 20–30% non-native short-chain lipids or detergents, which have the potential to affect the properties of the membrane as well as the protein.

Furthermore, the dense network of ¹³C–¹³C DCs, present in stationary samples of uniformly ¹³C/¹⁵N labeled proteins, is problematic, because it interferes with direct ¹³C detection²³ and with the execution of many other solid-state NMR experiments.^{23,24} Although, triple-resonance experiments are being developed to address this problem,^{25–28} they are not yet ready for application to uniformly ¹³C/¹⁵N labeled proteins. Proteins labeled uniformly only with ¹⁵N do not suffer from these limitations because of the spatial isolation and relatively low gyromagnetic ratio of the ¹⁵N nuclei in backbone amide sites.²⁹ It is also possible to alleviate this problem by using protein samples where the ¹³C nuclei are diluted and randomly isolated among all sites.^{23,24,30} However, isotopic dilution also reduces the gains in sensitivity obtained from direct ¹³C detection compared to ¹⁵N detection and attenuates the homonuclear DCs among proximate carbons that provide opportunities for making resonance assignments.

In contrast, MAS of uniformly ¹³C labeled proteins averages out the interfering homonuclear ¹³C–¹³C DCs, enabling direct ¹³C detection for high sensitivity as well as the implementation of ¹H/¹³C/¹⁵N triple-resonance pulse sequences for resonance assignments and measurements of structural restraints based on distances and dihedral angles. Recent developments in hardware and pulse sequences³¹ have enabled high-resolution MAS spectra to be obtained and assigned for a variety of polypeptides, including several membrane proteins in phospholipid proteoliposomes,^{32–37} proteolipid precipitates,^{38–40} lipid nanodiscs,⁴¹ and two-dimensional crystals.^{42–44} However, the measurement of a sufficient number of accurate structural restraints from the MAS spectra of uniformly ¹⁵N/¹³C labeled membrane proteins is challenging. Compared to the high precision and accuracy of orientation restraints measured in OS solid-state NMR spectra, distance restraints derived from spin diffusion under MAS are qualitative or have substantial uncertainties, although this is compensated by the large number of measurements that are made for each residue to generate high-resolution structures. Furthermore, their measurement is complicated by the prevalence of hydrophobic amino acids in membrane proteins. Rotational echo double-resonance^{45,46} experiments provide very accurate distances, but require the strategic placement of isotope label pairs by chemical synthesis or mutagenesis.

Following their initial demonstrations in the earliest stages of the development of high-resolution solid-state NMR of proteins, MAS^{29,47} and OS⁷ solid-state NMR methods have progressed,

for the most part, along separate paths. Here we describe how they can be reunited into a more powerful approach for structure determination of membrane proteins, by the inherent rapid diffusion of proteins around the bilayer normal.^{48,49} We demonstrate that this approach is capable of precisely determining the three-dimensional backbone structure of a membrane protein with two transmembrane helices.

The single line frequencies observed in the OS solid-state NMR spectra of uniaxially aligned samples are equivalent to the frequencies measured from the edges of motionally averaged powder patterns that result when proteins undergo uniaxial diffusion at a rate faster ($>10^5$ Hz) than the static spin interaction tensor. This equivalence was first demonstrated by McLaughlin and co-workers using ³¹P NMR of phospholipids.⁵⁰ An early experiment by Griffin and co-workers⁵¹ demonstrated that ¹³CO labeled bacteriorhodopsin, incorporated in phospholipid liposomes, undergoes rotational diffusion around the lipid bilayer normal and that lowering the sample temperature slows the diffusion sufficiently to enable the static powder pattern to be observed. We have obtained similar results for a transmembrane helical polypeptide labeled with ¹⁵N at a single backbone amide site,⁵² for other helical proteins with as many as seven transmembrane helices,⁵³ and for a β -barrel membrane protein.⁵⁴ In addition, there are many examples where rotationally averaged powder patterns have been used to ascertain the alignment of helices, sheets, and small peptides in bilayers.^{22,55–57} Recently, we have shown experimentally that the orientation-dependent frequencies measured from such rotationally aligned proteoliposomes are the same as those from magnetically aligned and glass-aligned lipid bilayer samples.⁵⁸ These results demonstrate that both the phospholipids and proteins undergo rotational diffusion around the bilayer normal, rapidly enough ($>10^5$ Hz) to average the static CSA and DC interactions into axially symmetric powder patterns with reduced frequency spans. Since the direction of rotation is parallel to the lipid bilayer normal, the sign and breadth of the resulting powder patterns reflect the angle between the principal axes of the relevant spin-interaction tensors and the lipid bilayer normal.

Recently developed pulse sequences enable recoupling of CSA and DC powder patterns under MAS.^{59–61} Here we demonstrate that these experiments can be used to recouple motionally averaged powder patterns resulting from a ¹⁵N/¹³C labeled membrane protein undergoing uniaxial rotational diffusion in phospholipid liposomes. The ¹H–¹³C DC, ¹H–¹⁵N DC, ¹³C CSA, and ¹⁵N CSA frequencies measured from the edges of these powder patterns provide orientation-dependent structural restraints for ¹³C α (CA), ¹³C' (CO), and ¹⁵N amide (N) protein sites. Building upon the physical foundation of measuring orientation restraints from motionally averaged powder patterns, we have developed an approach⁶² for determining the three-dimensional structures of membrane proteins in phospholipid bilayers. We illustrate it here by determining the backbone structure of MerFt, the 60-residue integral membrane core of the membrane protein transporter MerF from the bacterial mercury detoxification *mer* operon,⁶³ whose structure we have previously determined in both micelles⁶⁴ and magnetically aligned bilayers.¹²

This approach eliminates the limitations on samples by combining the measurement of orientation restraints for precise structure determination with MAS solid-state NMR resonance assignments. The principal spectroscopic benefits result from combining essential aspects of OS and MAS solid-state NMR with the use of uniformly ¹³C/¹⁵N labeled proteins embedded

in liquid crystalline proteoliposomes. Advantages over conventional OS solid-state NMR include the use of unoriented proteoliposome samples and the application of triple-resonance experiments to uniformly $^{13}\text{C}/^{15}\text{N}$ labeled proteins, which improves sensitivity through the use of direct ^{13}C (instead of ^{15}N) detection, permits the implementation of systematic assignment schemes among proximate sites, and provides signals from essentially all backbone and side chain sites for complete three-dimensional structure determinations. Furthermore, the use of only long-chain phospholipids in the samples has substantial advantages: it greatly simplifies sample preparation and data interpretation, it provides a more natural environment for the study of membrane proteins, and it enables a much greater variety of phospholipids to be used—virtually any bilayer-forming lipid—potentially including intact biological membranes.⁶⁵

EXPERIMENTAL METHODS

Protein Expression and Purification. MerFt, spanning residues 13–72 of the wild-type 81-residue MerF, was prepared essentially as described previously.^{12,64} It was expressed in inclusion bodies as a C-terminal fusion to ketosteroid isomerase (KSI) with a C-terminal His tag (KSI–MerFt–6His) in C43 (DE3) *Escherichia coli* cells (Overexpress, www.overexpress.com) grown on M9 minimal media containing ^{15}N labeled ammonium sulfate and uniformly $^{13}\text{C}_6$ labeled glucose (Cambridge Isotope Laboratories, www.isotope.com). After isolation of the inclusion bodies, the fusion protein was solubilized in 35 mM sodium dodecyl sulfate (SDS), 10 mM phosphate buffer (pH 7.4) and purified using Ni–NTA (nitrilotriacetic acid) Superflow resin (Qiagen, www.qiagen.com). Following elution with 0.1 M imidazole, MerFt was cleaved from KSI and from the His tag by treatment with cyanogen bromide in 70% formic acid and was purified to homogeneity by size exclusion chromatography on Sephacryl S-200 (GE Biosciences, www.gelifesciences.com) in 35 mM SDS, 100 mM phosphate buffer (pH 7.4). The protein was extensively dialyzed against water to remove all SDS and then lyophilized for storage. The purified protein migrates a single band on SDS–PAGE (polyacrylamide gel electrophoresis) (Figure 1), with an apparent molecular weight corresponding to the monomeric polypeptide and no evidence of aggregation or impurities.

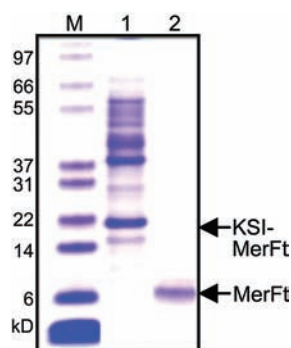


Figure 1. SDS–PAGE of purified MerFt: (M) molecular weight marker, (lane 1) inclusion bodies isolated from bacteria expressing the target protein as a fusion protein with KSI, (lane 2) purified protein after Ni–NTA affinity and size exclusion chromatographies. The arrows mark the positions of the designated polypeptides.

For reconstitution in dimyristoylphosphatidylcholine (DMPC) liposomes, 3.6 mg of MerFt was dissolved in a solution of 50% water, 49.9% trifluoroethanol (TFE), and 0.1% trifluoroacetic acid (TFA) and then centrifuged (7200g) for 2 min at 4 °C to remove insoluble material. The supernatant was passed through a 0.2 μm filter, dried under a stream of nitrogen gas, and then lyophilized to remove any residual water. The lyophilized protein was dissolved in 500 μL of neat TFE and mixed with 12 mg of DMPC dissolved in 500 μL of neat chloroform. The sample was dried under nitrogen gas and then

lyophilized. The MerFt/DMPC mixture was suspended in 5 mL of 10 mM 2-(*N*-morpholino)ethanesulfonic acid (MES) buffer (pH 6.1) and centrifuged (39000g, Beckman Ti 70.1 rotor) overnight at 15 °C. The supernatant was discarded, and then the hydrated proteoliposome pellet was packed into a 3.2 mm rotor.

Lipid Analysis. To quantitatively monitor the phospholipid and any residual detergent content of the proteoliposomes, HPLC analysis was performed using an evaporative light scattering detection system (Sedex 75, www.sedere.com). A LiChrosphere 100 NH_2 column (Merck, www.merck-chemicals.com) was used with a mobile phase composed of 70% acetonitrile, 20% methanol, and 10% 0.1 M ammonium acetate (pH 4.8). The samples were diluted in the running buffer before being loaded onto the column. After column separation, the analytes were evaporated under a stream of nitrogen gas, and the nonvolatile components were detected by light scattering. The photomultiplier signal is nearly linearly proportional to the analyte concentration. The final sample contained only DMPC and no SDS, within the detection limits, which are much less than 1%.

NMR Spectroscopy. Solid-state NMR experiments were performed on a 750 MHz Bruker Avance spectrometer equipped with a Bruker low-*E* $^1\text{H}/^{13}\text{C}/^{15}\text{N}$ triple-resonance 3.2 mm MAS solid-state NMR probe. The rotor sample volume was $\sim 30 \mu\text{L}$. The spinning rate was controlled to $11.11 \text{ kHz} \pm 2 \text{ Hz}$ using a Bruker MAS controller. The sample temperature was maintained as $25 \pm 2 \text{ }^\circ\text{C}$ in all experiments. During direct ^{13}C detection, 100 kHz radio frequency (rf) irradiation was used for ^1H decoupling with swept frequency two-pulse phase modulation (SW-TPPM),⁶⁶ and 2.5 kHz rf irradiation with WALTZ-16⁶⁷ was used for ^{15}N decoupling. Cross-polarization (CP)⁶⁸ from ^1H to ^{15}N was optimized using amplitude-modulated rf irradiation (100–50%) applied on the ^1H channel; 50 kHz rf irradiation on the ^1H and $\sim 27 \text{ kHz}$ rf irradiation on the ^{15}N channels were applied during the 1 ms contact time. Double CP was accomplished by transferring magnetization from ^{15}N amide to ^{13}C using spectrally induced filtering in combination with cross-polarization (SPECIFIC-CP).⁶⁹ Adiabatic tangential pulses were applied on the ^{13}C channel. Typically, rf irradiations of $\sim 27 \text{ kHz}$ were applied on the ^{15}N channel and $\sim 16 \text{ kHz}$ on the ^{13}C channel for band-selective polarization transfer. SW-TPPM decoupling with 100 kHz radio frequency irradiation was applied during the double CP transfer. ^{15}N to ^{13}C polarization transfer was accomplished using proton-assisted insensitive nuclei CP (PAIN-CP).⁷⁰ A 50 kHz continuous wave (CW) rf irradiation was applied on the ^{13}C and ^{15}N channels and 62 kHz CW rf irradiation to the ^1H channels for spin locking during PAIN-CP. The ^{13}C rf irradiation was placed at 175 ppm during PAIN-CP. Slow spinning (5 kHz) MAS spectra were obtained using a 4 μs 90° pulse for direct ^{13}C excitation followed by a Hahn spin echo with a 400 μs delay under ^1H irradiation prior to ^{13}C detection. The chemical shift frequencies were referenced externally to the adamantane methylene ^{13}C resonance at 38.48 ppm and the ammonium sulfate ^{15}N resonance at 26.8 ppm.

Resonance assignments were made using two- and three-dimensional correlation experiments, including $^{13}\text{C}/^{13}\text{C}$ homonuclear spin exchange, nitrogen $\text{C}\alpha$ carbonyl (NCACO) and nitrogen carbonyl $\text{C}\alpha$ (NCOCA). Two-dimensional $^{13}\text{C}/^{13}\text{C}$ correlation experiments were performed under proton-driven spin diffusion (PDSD)^{71–73} with 50 and 450 ms mixing periods. The 50 ms mixing period provides one-bond correlations, and the 450 ms mixing period provides total intraresidue and inter-residue correlation. Experiments were performed using ^1H to ^{13}C CP. For ramped-amplitude CP (RAMP-CP), the amplitude of the ^1H radio frequency irradiation was modulated to maximize the transfer, and a 100 μs spin-lock period on both channels was used to selectively polarize only the proton-bearing carbons. Other pertinent experimental parameters were 128 scans, 2 s recycle delay, and 10 and 4.6 ms ^{13}C chemical shift evolution periods in the direct and indirect dimensions. In the three-dimensional NCACO experiment, $^{13}\text{C}/^{13}\text{C}$ correlation was achieved with PDSD with 50 ms mixing. In the three-dimensional NCOCA experiment, $^{13}\text{C}/^{13}\text{C}$ correlation was achieved with dipolar assisted rotational resonance (DARR)⁷⁴ using a 20 ms mixing period. The three-dimensional NCOCA spectra have more cross-peaks due to long-range correlations established under the PAIN CP conditions. The experimental conditions included 10 ms carbon

evolution in the direct dimension, 2.88 ms ^{13}C and ^{13}CO chemical shift evolution, and 5.76 ms ^{15}N amide chemical shift evolution for the three-dimensional experiments.

Three-dimensional ROCSA⁵⁹ experiment was used to measure the ^{15}N sites CSA powder patterns associated with individual ^{15}N amide and ^{13}C isotropic chemical shifts in three orthogonal dimensions using $\text{C}2_2$ symmetry pulses,^{59,75} a 180 μs dwell time, and 24 complex points, collected during the CSA recoupling period. A 2.16 ms evolution period for ^{13}C and a 5.76 ms period for ^{15}N were used during CSA recoupling in the three-dimensional experiments.

Two-dimensional ^{13}C -detected separated local field (SLF) experiments that correlate ^1H - ^{15}N DC frequencies with ^{13}C isotropic chemical shifts were performed in three steps (Figure 2). First, ^{15}N

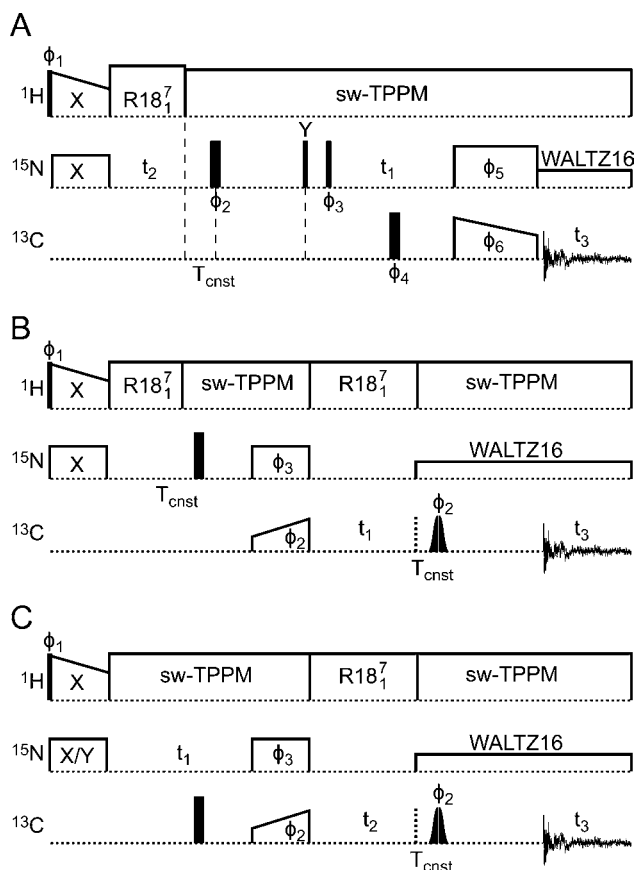


Figure 2. Schematic timing diagrams for the pulse sequences used to obtain multidimensional SLF spectra with ^{13}C detection: (A, C) three-dimensional SLF experiments that correlate ^{15}N and ^{13}C isotropic chemical shift frequencies with ^1H - ^{15}N DC and ^1H - ^{13}C DC frequencies, respectively, (B) three-dimensional SLF experiment that correlates ^1H - ^{15}N DC and ^1H - ^{13}C DC frequencies with the ^{13}C isotropic chemical shift frequency.

magnetization was generated by cross-polarization from ^1H prior to dipolar evolution. Second, ^1H - ^{15}N dipolar evolution was carried out under $\text{R}18_1$ symmetry pulse sequences to assist in the simultaneous recoupling of heteronuclear DC and decoupling of homonuclear DC.⁷⁶ ^1H - ^{15}N DC frequencies were encoded in a constant time manner with refocusing of ^{15}N chemical shifts and rapid dephasing of the ^{13}C signals. Third, after dipolar evolution, ^{15}N magnetization was transferred to ^{13}C using SPECIFIC-CP,⁷⁷ and the ^{13}C signals were acquired with ^1H decoupling. Three-dimensional experiments were carried out in similar fashion with incorporation of a ^{15}N chemical shift evolution period in the third dimension.

A two-pulse phase modulation with 70° and -70° phases for each pulse length of 5 μs was used in the $\text{R}18_1$ cycle. Nine repetitions of the paired pulses over one rotor period and a dwell time of 90 μs

were used in the indirect dimension to observe dipolar evolution. Refocusing periods of 4.8 and 3 ms were used in the constant time (T_{cnst}) echo for the ^1H - ^{15}N and ^1H - ^{13}C dipolar evolutions, respectively. A 10 μs hard pulse and 180 μs Gaussian selective 180° pulse were used for refocusing of ^{15}N and ^{13}C chemical shift frequencies, respectively. A total of 2.34 ms for ^1H - ^{15}N DC evolution and 1.44 ms for ^1H - ^{13}C DC evolution were used in the SLF experiments. Following the dipolar evolution period, a 3.6 ms z-filter was incorporated to cancel any antiphase magnetization evolution. Quadrature detection in the indirect dimension used to measure the ^{15}N chemical shift evolution was accomplished in a States mode⁷⁸ by incrementing the phase of the ^{15}N CP spin-lock pulses shown in Figure 2C or the 90° pulse phase ϕ_3 in Figure 2A.

Three-dimensional $^1\text{H}/^{15}\text{N}$ SLF data were acquired using the pulse sequence shown in Figure 2A with evolution periods of 10 ms for the ^{13}C chemical shift, 5.76 ms for the ^{15}N chemical shift, and 2.34 ms for ^1H - ^{15}N DC. Similarly, experiments with 1.44 ms ^1H - ^{13}C dipolar evolution periods were used to obtain three-dimensional $^1\text{H}/^{13}\text{C}$ SLF data using the pulse sequence in Figure 2C. The three-dimensional experiment in Figure 2B was used to correlate the ^1H - ^{15}N and ^1H - ^{13}C dipolar frequencies associated with a single ^{13}C chemical shift frequency using 10 ms for the ^{13}C chemical shift evolution and 1.08 ms for ^1H - ^{13}C and 1.44 ms for the ^1H - ^{15}N dipolar coupling evolution periods.

Structure Calculations. Structure calculations were performed in two stages. First, a starting structural model of the protein was generated with Rosetta,^{79,80} and second, the model was refined against the NMR restraints using XPLOR-NIH⁸¹ to yield the final refined structure of the protein. Molecular structures were analyzed and visualized with Pymol.⁸²

The amino acid sequence of MerFt together with the assigned backbone isotropic chemical shifts were used to generate three- and nine-residue fragments on the Robetta server.⁸³ Fifty-two ^1H - ^{15}N DC restraints were used to fold 10 000 structural decoys using the membrane ab initio protocol in Rosetta 3.2.⁸⁰ The lowest energy Rosetta-generated structural model was selected as the starting point for refinement against the experimental restraints in XPLOR-NIH.

Structure refinement was performed using a simulated annealing protocol consisting of a 10 ps torsion angle molecular dynamics phase at a temperature of 1500 K, followed by simulated annealing from 1500 to 20 K in 10 K increments at each step of 0.2 ps torsion-angle molecular dynamics.⁸⁴ Finally, gradient minimization was performed in Cartesian coordinates. The structure was refined against 52 ^1H - ^{15}N DC restraints, imposed with a force constant ramped from 0.2 to 2 $\text{kcal}\cdot\text{mol}^{-1}\cdot\text{kHz}^{-2}$, 28 ^1H - ^{13}C DC restraints with a force constant ramped from 0.01 to 0.5 $\text{kcal}\cdot\text{mol}^{-1}\cdot\text{Hz}^{-2}$, 42 ^{15}N amide CSA restraints with a force constant ramped from 0.05 to 0.5 $\text{kcal}\cdot\text{mol}^{-1}\cdot\text{ppm}^{-2}$, and 110 Rosetta-derived backbone dihedral angle (ϕ , ψ) restraints with a force constant ramped from 200 to 500 $\text{kcal}\cdot\text{mol}^{-1}\cdot\text{rad}^{-2}$. In addition, the knowledge-based torsion angle potential of mean force⁸⁵ was included as well as energy terms to enforce covalent geometry and prevent atomic overlap.⁸⁶ A total of 100 structures were calculated using XPLOR-NIH, and the 20 lowest energy structures were accepted for analysis.

Values of the ^1H - ^{15}N DC, ^1H - ^{13}C DC, and ^{15}N CSA used in the structure calculations were derived from the experimentally measured perpendicular edge frequencies of the respective rotationally averaged powder patterns. For DC, the perpendicular edge frequencies were multiplied by 4 to obtain the full DC value, corresponding to twice the parallel edge frequency. For ^{15}N CSA, the anisotropic perpendicular edge frequency was first reduced to its traceless value by subtracting the experimentally measured isotropic ^{15}N chemical shift and then multiplied by 2 to obtain the full CSA frequency span. In most measurements, the sign of the ^1H - ^{15}N DC could be determined unambiguously. In those cases where this was not possible, and for all of the ^1H - ^{13}C DC data, the DC restraints were implemented as absolute values in the energy calculation. During simulated annealing, the magnitude and symmetry of the molecular alignment tensor were fixed, with values of the axial alignment parameter (Da) and rhombicity (Rh) set to 10.52 kHz and 0, respectively, as expected for a membrane protein in phospholipid bilayers with an order parameter

of ~ 1.0 and an amide NH bond length of ~ 1.05 Å. In the calculations, the ^1H - ^{13}C DC and the ^{15}N amide CSA alignment tensors were normalized to the maximum value of the ^1H - ^{15}N DC. The traceless values and the molecular orientation of the ^{15}N amide chemical shift tensor were $\delta_{11} = -42.3$ ppm, $\delta_{22} = -55.3$ ppm, $\delta_{33} = 97.7$ ppm, $\beta = 17^\circ$, and $\gamma = 0^\circ$ for non-Gly residues and $\delta_{11} = -41.3$ ppm, $\delta_{22} = -64.3$ ppm, $\delta_{33} = 105.7$ ppm, $\beta = 20^\circ$, and $\gamma = 0^\circ$ for Gly residues.⁸⁷

The NMR and structure refinement statistics are provided in Table S1, Supporting Information. Atomic coordinates, resonance assignments, and NMR restraints have been deposited in the Protein Data Bank (PDB 2LJ2). NMR assignments have been deposited in the Biological Magnetic Resonance Bank (BMRB 17914).

RESULTS AND DISCUSSION

MerF⁸⁸ transports Hg(II) from the periplasm into the cell cytoplasm where it is reduced by the enzyme mercuric reductase to the less toxic and volatile Hg(0) as an essential part of the bacterial mercury detoxification system. Previously, we determined the three-dimensional structure of MerFt, a 60-residue construct spanning the integral membrane helix–loop–helix region of MerF (81 residues), in micelles by solution NMR⁶⁴ and in magnetically aligned bilayers by OS solid-state NMR.¹² The mobile residues observed at the N- and C-termini of full-length MerF in micelles are absent in MerFt.⁶⁴

In OS solid-state NMR, the structures of membrane proteins are determined by measuring multiple single line frequencies that provide orientation restraints relative to a single-order axis, defined by the magnetic field. For membrane proteins incorporated in liposomes and undergoing fast rotational diffusion around the bilayer normal, the same orientation restraints can be obtained from the parallel edge frequencies of motionally averaged powder patterns, recoupled by MAS solid-state NMR experiments that simultaneously perform homonuclear decoupling of the ^{13}C – ^{13}C interactions, and the averaging that yields resonances with isotropic chemical shift frequencies. This enables all of the structural analysis methods developed for OS solid-state NMR to be applied to unoriented proteoliposomes containing uniformly $^{13}\text{C}/^{15}\text{N}$ labeled proteins.

Rapid rotational diffusion of the protein around a single axis, at a rate faster than the frequency breadth of the static powder patterns, is essential for this solid-state NMR approach. In early studies, rotational diffusion was observed in a wide variety of proteins by several biophysical techniques,^{48,49} and NMR studies have shown that both lipids and many membrane proteins undergo rotational diffusion in bilayer membranes.^{22,50–58}

In helical membrane proteins, a large fraction of the backbone carbonyl bonds are aligned along helix axes as they participate in hydrogen bonds with amide NH groups. For transmembrane helices this means that most CO bonds are approximately parallel to the bilayer normal (i.e., the axis of motional averaging). Thus, fast protein rotation around the bilayer normal results in a significantly narrowed, symmetric ^{13}C CSA powder pattern (Figure 3A); by contrast, the static powder pattern is highly asymmetric and has a large frequency span (Figure 3B). The $\sim 10^5$ Hz frequency cutoff for obtaining a motionally averaged powder pattern is defined by the frequency spans (kHz) of the static powder patterns for the ^1H - ^{13}C CA and ^1H - ^{15}N amide DC and the ^{13}C , ^{13}C CA, and ^{15}N amide CSA interactions and will vary somewhat with the field strength of the magnet used for the experiments.

To verify that MerFt undergoes rotational diffusion on this time scale, and that diffusion can be switched between the slow and fast limits, we monitored the ^{13}C CSA powder pattern in a uniformly $^{13}\text{C}/^{15}\text{N}$ labeled sample of the protein at

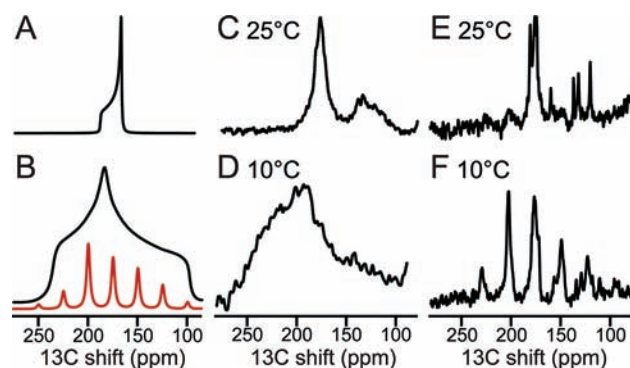


Figure 3. ^{13}C solid-state NMR spectra of uniformly $^{13}\text{C}/^{15}\text{N}$ labeled MerFt in DMPC proteoliposomes. The majority of resonance intensity centered near 175 ppm is from ^{13}C backbone sites. (A, B) Spectra simulated for a single ^{13}C group in a transmembrane helix undergoing rotational diffusion around the lipid bilayer normal. The family of sidebands in panel B (red) would be observed under MAS. (C, D) Spectra obtained for a stationary sample, at 25 °C, where the protein undergoes fast rotational diffusion about the phospholipid bilayer normal, or at 10 °C, where the protein is immobile on the time scale of the static ^{13}C CSA powder pattern ($\sim 10^5$ Hz). (E, F) Spectra obtained from a sample undergoing slow (5 kHz) MAS, at 25 °C, where the ^{13}C CSA powder pattern is motionally averaged, or at 10 °C, where a family of sidebands spanning the width of the static ^{13}C CSA powder pattern is observed in the absence of protein rotational diffusion. Comparisons of the powder pattern frequency breadth (A versus B; C versus D) or the presence of spinning sidebands (E versus F) are diagnostic for the presence of fast rotational diffusion of the protein under the experimental conditions used to measure the CSA and DC powder patterns.

temperatures below (10 °C) or above (25 °C) the gel to liquid crystalline phase transition temperature of the DMPC phospholipid bilayer. The powder pattern obtained at 10 °C, where the bilayer is in the gel phase, spans the full width of the ^{13}C CSA, with no evidence of motional averaging (Figure 3D). In contrast, the powder pattern obtained at 25 °C, where the lipid bilayer is liquid crystalline, is fully rotationally averaged (Figure 3C). MerFt begins to undergo rotational diffusion, fast enough to affect the static powder pattern, at temperatures above ~ 17 °C, since the phase transition temperature of DMPC is reduced by the presence of the protein. At 25 °C, two distinguishable bands of resonance intensity are present in the spectrum. The signal intensity centered at 120 ppm is attributed to the aromatic side chain carbons and that centered at 175 ppm to the backbone ^{13}C sites. The dramatic reduction in the breadth of the ^{13}C powder pattern observed upon raising the temperature through the lipid phase transition demonstrates experimentally that, at 25 °C, the protein undergoes rotational diffusion faster than the 10^5 Hz required to average the static powder patterns.

Under conditions of relatively slow (5 kHz) MAS, there are no spinning sidebands apparent in the 25 °C spectrum (Figure 3E). This is consistent with the ^{13}C CSA powder pattern having a small frequency span due to the averaging effects of uniaxial rotational diffusion. By contrast, the MAS solid-state NMR spectrum obtained at 10 °C (Figure 3F) has a family of spinning sidebands flanking the center band at 175 ppm, demonstrating that the ^{13}C CSA powder pattern has a large frequency span at 10 °C where the protein does not undergo rotational diffusion fast enough to average the ^{13}C CSA. This is also

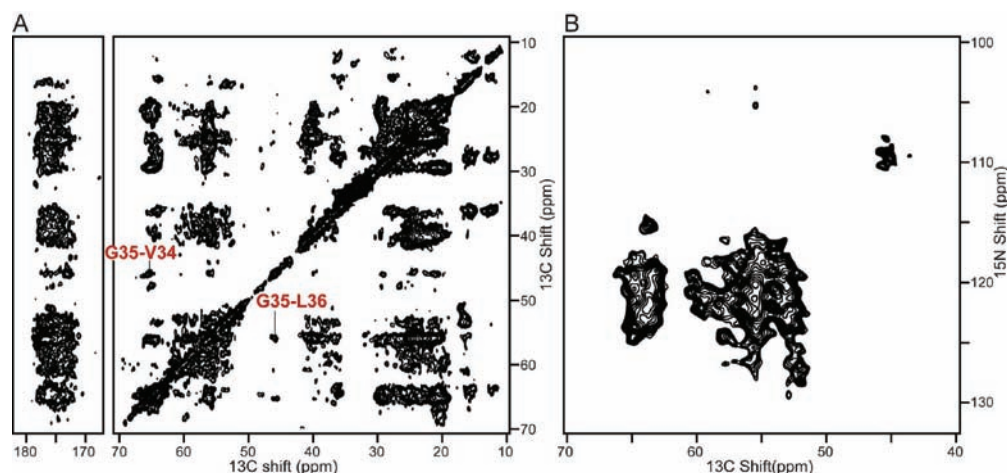


Figure 4. Two-dimensional MAS spectra of uniformly $^{13}\text{C}/^{15}\text{N}$ labeled MerFt in DMPC proteoliposomes at 25 °C: (A) homonuclear $^{13}\text{C}/^{13}\text{C}$ spin-exchange correlation spectrum, (B) heteronuclear $^{13}\text{C}/^{15}\text{N}$ correlation spectrum. The experiments were performed at 750 MHz under 11.11 kHz MAS.

illustrated with the simulated spectrum corresponding to these MAS conditions (Figure 3B, red).

Powder pattern line shapes can be reconstructed from the intensities of the spinning sidebands observed in MAS solid-state NMR spectra, as shown in Figure 3B.⁸⁹ The magnitudes of the principal elements and the asymmetry of the ^{13}C CSA powder patterns observed under stationary and slow MAS conditions are for all practical purposes the same. At 25 °C, both stationary (Figure 3A,C) and MAS (Figure 3E) spectra show a drastic narrowing of the frequency span due to the protein's uniaxial rotational diffusion. Although all of the ^{13}C sites have similar isotropic chemical shifts, some (e.g., those in structured interhelical loops or terminal regions) have orientations relative to the bilayer normal quite different from those of residues in transmembrane helices; as a result, it is difficult to obtain reliable measurements of their frequency spans or asymmetries from one-dimensional spectra. Nonetheless, because helical membrane proteins are characterized by having a majority of ^{13}C groups in transmembrane helices, approximately parallel to the bilayer normal, direct comparison of the ^{13}C CSA powder patterns obtained below and above the lipid phase transition is generally sufficient to demonstrate that a membrane protein undergoes fast rotational diffusion in lipid bilayers. In this way, we have observed fast rotational diffusion of six different helical membrane proteins, with between one and seven transmembrane helices, and of a β -barrel protein in DMPC bilayers at temperatures near 25 °C.

Two- and three-dimensional spectra were used to resolve signals from individual protein sites and to provide the foundations for the crucial assignment and recoupling MAS solid-state NMR experiments. Two-dimensional $^{13}\text{C}/^{13}\text{C}$ dilute-spin-exchange spectra^{71–73} and $^{13}\text{C}/^{15}\text{N}$ heteronuclear correlation spectra⁷⁷ are useful starting points; for a small protein, such as MerFt, they provide resolution of signals from nearly all sites (Figure 4). Furthermore, uniform $^{13}\text{C}/^{15}\text{N}$ isotopic labeling of the protein enables direct transfers of magnetization through DCs in the backbone. This provides a mechanism for correlating the isotropic chemical shift frequencies of directly bonded ^{13}C and ^{15}N nuclei. Using a combination of homonuclear two-dimensional and triple-resonance two- and three-dimensional MAS solid-state NMR experiments, we were able to assign the backbone resonances of MerFt in proteoliposomes at 25 °C. Representative

connecting strips used to make the resonance assignments are shown in Figure 5, and the complete set for all residues in the protein is shown in Figure S1, Supporting Information.

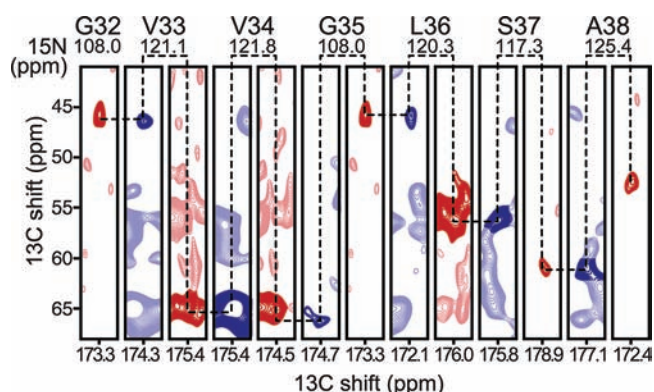


Figure 5. Representative strip plots for residues G32–A38 of uniformly $^{13}\text{C}/^{15}\text{N}$ labeled MerFt in DMPC proteoliposomes at 25 °C. The spectral strips were extracted from MAS three-dimensional NCACO (red) and NCOCA (blue) spectra. Both experiments were performed at 750 MHz under 11.11 kHz MAS. Dashed lines have been added to guide the eye through the backbone resonance walk.

The connections between CA_i and CO_i chemical shift frequencies (for residue i) are encoded in the intraresidue $\text{N}_i\text{CA}_i\text{CO}_i$ spectra by the inter-residue $\text{N}_{i+1}\text{CO}_i\text{CA}_i$ experiments. This provides an efficient means for identifying amide pairs in neighboring residues. In cases of spectral overlap, it is advantageous to use the $\text{CA}_i\text{--CA}_{i+1}$ correlations observable in two-dimensional $^{13}\text{C}/^{13}\text{C}$ PDSO or three-dimensional NCACX experiments performed under conditions where long-range inter-residue correlations are observable. For example, the inter-residue connectivity between the ^{13}C chemical shifts of Gly35 and Leu36 and Val34 are marked in the two-dimensional $^{13}\text{C}/^{13}\text{C}$ correlation spectrum in Figure 4A. The ^{13}C resonance from the following residue is useful in eliminating any remaining ambiguities. Additionally, when three-dimensional NCACX data are available, side chain resonance patterns can often be observed in the direct CX dimension, enabling residue types to be identified through the statistical evaluation of their $^{13}\text{C}/^{15}\text{N}$ chemical shift values.⁹⁰

To characterize the rotationally averaged DC and CSA powder patterns associated with each resolved isotropic resonance, we implemented three-dimensional MAS solid-state NMR recoupling experiments. The three multidimensional experiments outlined in Figure 2 provide both the spectral resolution and recoupling of powder patterns required to detect and characterize signals from individual sites.

The two-dimensional ^1H - ^{15}N DC/ ^{13}C shift SLF spectrum of MerFt (Figure 6A) contains resonances from all ^{13}C sites.

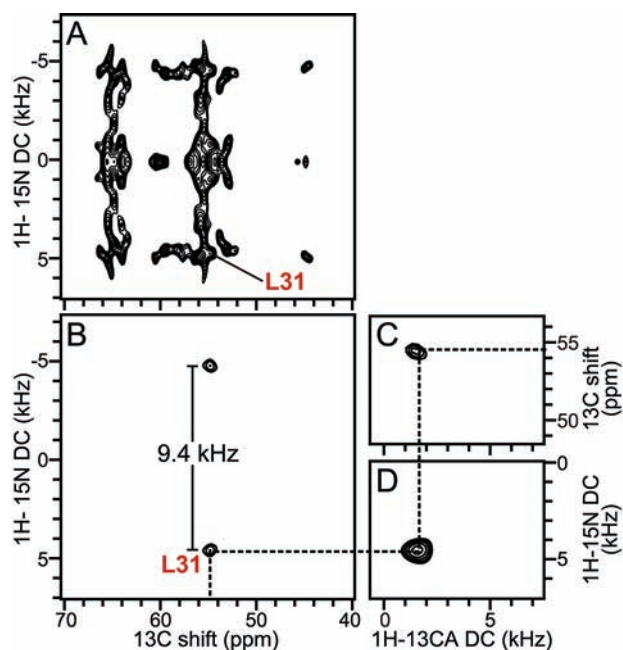


Figure 6. Examples of spectroscopic data for residue L31 obtained from MAS solid-state NMR spectra of uniformly $^{13}\text{C}/^{15}\text{N}$ labeled MerFt in DMPC proteoliposomes at 25 °C: (A) two-dimensional ^1H - ^{15}N DC/ ^{13}C shift SLF spectrum, (B) two-dimensional ^1H - ^{15}N DC/ ^{13}C shift SLF spectral plane selected from a three-dimensional spectrum at an isotropic ^{15}N chemical shift frequency of 118.6 ppm, (C) two-dimensional ^1H - ^{13}C DC/ ^{13}C shift SLF spectral plane selected from a three-dimensional spectrum at an isotropic ^{15}N chemical shift frequency of 118.6 ppm, (D) two-dimensional ^1H - ^{13}C DC/ ^1H - ^{15}N DC SLF spectral plane selected from a three-dimensional spectrum at an isotropic ^{13}C chemical shift frequency of 54.6 ppm. All three spectral planes are associated with residue L31. The dashed line traces the correlation among the frequencies, which were obtained from three separate experiments using the pulse sequences diagrammed in Figure 2. The DC frequencies in the spectra correspond to the perpendicular edge frequencies of the corresponding powder patterns. Panel B shows that the ^1H - ^{15}N DC motionally averaged powder pattern for L31 has a perpendicular edge frequency of 4.7 kHz, corresponding to a splitting of 9.4 kHz, and a DC value of 18.8 kHz.

Although there is considerable spectral overlap, the individual resonances assigned to Leu31 can be identified by comparison with the two-dimensional ^1H - ^{15}N DC/ ^{13}C shift SLF planes, selected from a three-dimensional ^{13}C -detected SLF spectrum at the ^{15}N chemical shift frequency of Leu31 (Figure 6B). These results were obtained with the pulse sequence diagrammed in Figure 2A. Similarly, values of the ^1H - ^{13}C DC were measured in three-dimensional experiments correlating ^{13}C and ^{15}N amide isotropic chemical shifts using the pulse scheme in Figure 2C. Two-dimensional planes extracted from these types of three-dimensional spectra are shown in Figure 6C,D for Leu31 of MerFt. Correlating ^1H - ^{13}C DC and ^1H - ^{15}N DC to a common

^{13}C isotropic chemical shift can often be used to lift degeneracies that occur when two or more sites have the same or very similar ^{13}C and ^{15}N isotropic chemical shift frequencies.

One-dimensional spectral slices, extracted from a three-dimensional data set at specific ^{13}C or ^{15}N isotropic chemical shifts, were used to measure the orientation-dependent frequencies that characterize the motionally averaged ^{15}N CSA, ^1H - ^{15}N DC, and ^1H - ^{13}C DC powder patterns for individual residues and serve as restraints in structure determination (Figure 7).

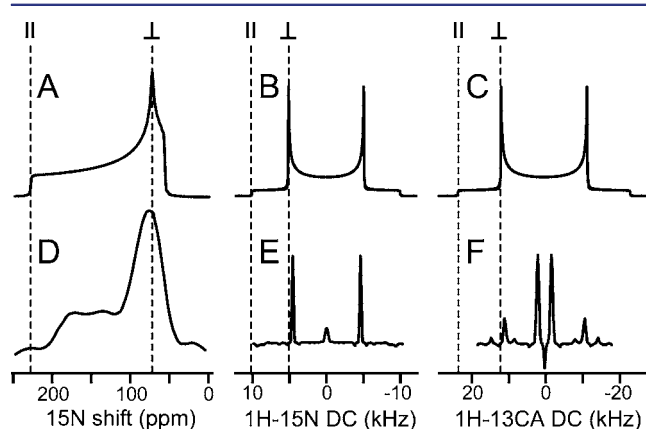


Figure 7. Examples of spectroscopic data for residue L31 obtained from MAS solid-state NMR spectra of uniformly $^{13}\text{C}/^{15}\text{N}$ labeled MerFt in DMPC proteoliposomes at 25 °C: (A–C) simulated powder patterns for a static peptide bond corresponding to (A) ^{15}N amide CSA, (B) ^1H - ^{15}N DC, and (C) ^1H - ^{13}C DC, (D–F) experimentally measured powder patterns recoupled under MAS. The dashed vertical lines mark the parallel (||) and perpendicular (⊥) edge frequencies. Values of the ^1H - ^{15}N DC and ^1H - ^{13}C DC measured from the perpendicular edge frequencies were multiplied by 4 to obtain the full DC values corresponding to twice the parallel edge frequency. For the ^{15}N CSA, the perpendicular edge frequency was reduced to its traceless value and then multiplied by 2 to obtain the full CSA value.

The data for Leu31 (Figure 7D–F) demonstrate that effective recoupling of the perpendicular edge frequencies (selected for their higher intensity) of the powder patterns is obtained. These are directly related to the full values of the DC and CSA, which are used in structure calculations.

Plotting the ^1H - ^{15}N DC values measured for each residue in MerFt as a function of the residue number yields a characteristic dipolar wave⁹¹ that enables helical segments of the protein to be readily identified and characterized with respect to the helix length, helix orientation in the membrane, and presence of any kinks. Notably, the ^1H - ^{15}N DC values measured here for MerFt in proteoliposomes (Figure 8B) are very similar to the values measured previously for the same protein in magnetically aligned bicelles¹² (Figure 8A), demonstrating that information obtained from motionally averaged powder patterns of proteins in liposomes, recoupled under MAS, is the same as that from single line OS solid-state NMR spectra of uniaxially aligned proteins.

The measured spectroscopic parameters were used to calculate de novo the three-dimensional structure of MerFt. The computational methods⁹² used to determine protein structures from orientation restraints are equally applicable to the frequencies measured from the edges of rotationally averaged powder patterns. For MerFt, structure calculation proceeded in two stages. First, Rosetta,^{79,80} in combination with measured values of the ^1H - ^{15}N DC and of backbone isotropic chemical

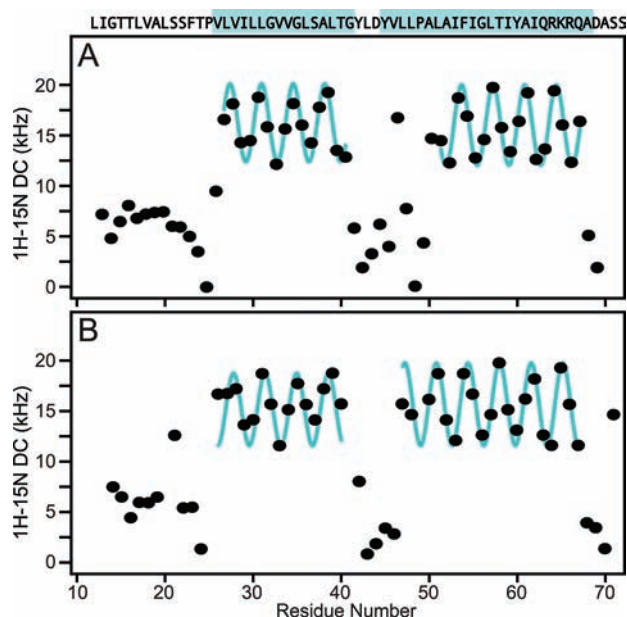


Figure 8. Dipolar waves obtained by plotting measured values of the ^1H - ^{15}N DC versus residue number for MerFt: (A) data from MerFt in magnetically aligned bicelles, directly measured from single resonance lines in OS solid-state NMR spectra,¹² (B) data from MerFt in un-oriented proteoliposomes, measured from motionally averaged powder patterns, recoupled under MAS. Sinusoidal fits (cyan) to the data trace the two transmembrane α -helices of the protein. (A) Reprinted from ref 12. Copyright 2006 American Chemical Society.

shifts, was used to generate initial structural models. Then the lowest energy Rosetta model was refined against all the experimental data by simulated annealing.

The resulting structure of MerFt (Figure 9) has an average backbone pairwise rmsd of ~ 1.2 Å (based on the 20 lowest

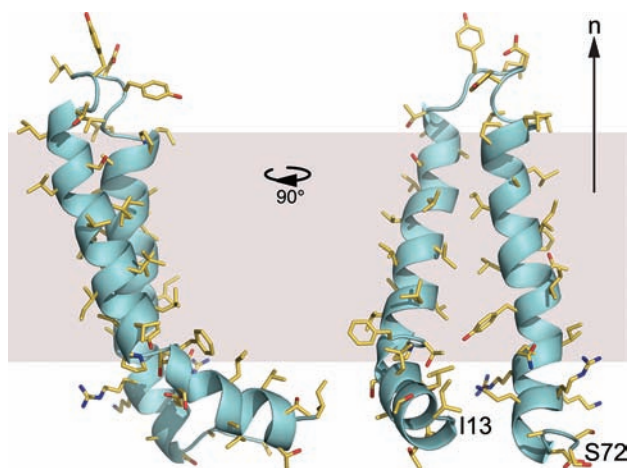


Figure 9. Three-dimensional structure of MerFt in DMPC phospholipid bilayers calculated from the experimental data. Both the protein structure and orientation are determined in the frame of the lipid bilayer membrane (gray) defined by the bilayer normal (n) in these calculations. The average pairwise rmsd for the 20 lowest energy structures is 1.2 Å for backbone atoms and 2.0 Å for all non-hydrogen atoms.

energy structures), no bond violations, and no angle violations greater than 7.5 Å (Table S1, Supporting Information). We are confident that these statistical parameters will improve with further advances of the experimental and calculation methods, as

they are applied to other membrane proteins in phospholipid bilayers, and by performing the structure refinement calculations in explicit lipid bilayer membranes rather than in vacuum, as described recently.¹³ For each MerFt residue, the experimentally measured values of the DC and CSA correlate remarkably well with the values calculated directly from the refined structure (Figure 10B–D), with a scatter reflecting primarily minor

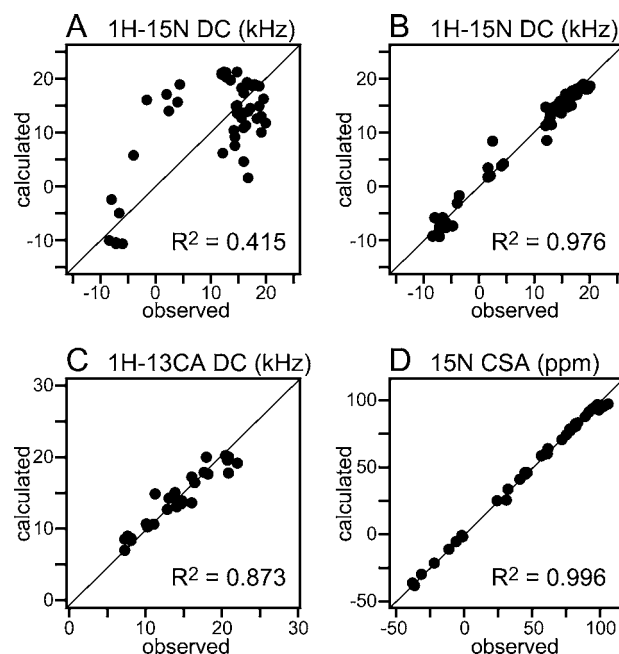


Figure 10. Correlations between observed and back-calculated values of orientation restraints used to calculate the structure of MerFt in phospholipid bilayers. (A) Calculated values were obtained from the initial Rosetta structural model. (B–D) Calculated values were obtained from the final refined structure. The R^2 correlation coefficient is listed for each type of restraint.

experimental errors in the measurements from spectra with limited signal-to-noise ratios are reduced. Refinement against the experimental restraints is highly effective, since the correlations improve dramatically from those obtained with the initial Rosetta structural model (Figure 10A) to those obtained after refinement against the experimentally measured orientation restraints (Figures 10B–D). We find that the correlation coefficients for these plots are highly reliable indicators of the quality of experimental structure determination, with high correlation coefficients generally reflecting low rmsd values.

In the resulting structure, the arrangement of the two transmembrane helices recapitulates the integral membrane topology of MerFt first determined in micelles⁶⁴ and magnetically aligned bilayers.¹² Refinement against the lipid bilayer normal provides not only the three-dimensional protein structure but also its three-dimensional orientation within the lipid bilayer membrane. Interestingly, the N-terminal amphipathic helix (Thr15 to Thr24) preceding the first transmembrane helix (Val26 to Gly41) adopts an orientation tending toward the membrane surface, with the hydrophobic residue facing the lipid membrane and polar residues facing the aqueous milieu. This is as expected for an amphipathic helix near the membrane–water interface and underscores the importance of determining membrane protein structures in their natural environment of the phospholipid bilayer, where such structural features are retained and can be identified. These details should be fully resolved

when the structure of the full-length wild-type MerF protein becomes available and by performing structure refinement in phospholipid bilayers.

CONCLUSIONS

The structure of MerFt was determined from a single proteoliposome sample containing 3.5 mg of uniformly $^{13}\text{C}/^{15}\text{N}$ labeled protein prepared by expression in bacteria. Structure determination was accomplished by combining key elements of OS solid-state NMR with MAS solid-state NMR methods.

The principal advantage of this approach is that all experiments were carried out with liquid crystalline proteoliposomes at 25 °C; thus, the resulting structure represents MerFt in membranes at close to physiological conditions of temperature and pH, an environment that is very close to native. In particular, detergents and other non-natural additives that have the potential to distort protein structure and function are avoided. Liposomes can be prepared with virtually any bilayer-forming phospholipid, enabling experiments to be performed just as easily with a lipid composition similar to that of the bacterial membrane where MerF is found naturally. In the future it may be possible to extend the method to proteins in intact cell membranes.⁶⁵ It is increasingly well-recognized that the surrounding membrane environment is important for preserving the structural and functional integrity of membrane proteins.⁹³ Structure determination of membrane proteins in natural settings provides access to fundamental biological processes that depend on an integral membrane environment for function (e.g., dynamics, conformational changes, and interactions with ligands, drugs, antibody fragments, and lipids).

Furthermore, a major advantage of combining OS with MAS solid-state NMR methods is the ability to use uniformly $^{13}\text{C}/^{15}\text{N}$ labeled proteins for high-resolution spectroscopy and resonance assignments, while retaining the ability to measure accurate orientation restraints for precise structure determination. The implementation of ^{13}C detection provides higher sensitivity, and the use of proteoliposomes circumvents the need for preparation and optimization of aligned samples. Since rotational diffusion is an inherent property of most membrane proteins embedded in membranes, this has the potential to be a general method for membrane protein structure determination. We do not know if there is a size limit for rotational diffusion in bilayers, but it is clearly present in membrane proteins with seven transmembrane helices, including bacteriorhodopsin⁵¹ and G-protein coupled receptors,⁵³ which are prime targets for structural studies.

Finally, this approach to structure calculation has the advantage that it relies on minimizing the difference between experimentally observed spectral frequencies and frequencies calculated from a starting structural model, made possible by the use of orientation restraints in combination with recent developments in bioinformatics model prediction methods such as Rosetta.^{79,80} Since the order tensor is predetermined by the sample geometry and the rotational diffusion of the protein around the lipid bilayer normal, the interpretation of spectral frequencies in terms of structural restraints is straightforward. The structure of MerFt was determined solely on the basis of orientation restraints and dihedral angles derived from bioinformatic analysis of isotropic chemical shifts. However, both structural accuracy and precision will be improved by including a few distance restraints, especially for proteins where the loops and terminal regions are substantially larger. Furthermore, extending the measurements to side chain sites, using a similar

strategy, offers a path to complete three-dimensional structure determination of membrane proteins.

ASSOCIATED CONTENT

Supporting Information

Table containing the structure determination statistics and additional experimental details. This material is available free of charge via the Internet at <http://pubs.acs.org>.

AUTHOR INFORMATION

Corresponding Author

sopella@ucsd.edu

ACKNOWLEDGMENTS

We thank Chris Grant and Albert Wu for assistance with the instrumentation and Charles Schwieters for assistance with XPLOR-NIH. This research was supported by grants from the National Institutes of Health and utilized the Biomedical Technology Resource for NMR Molecular Imaging of Proteins at the University of California, San Diego, supported by Grant P41EB02310.

REFERENCES

- (1) Wallin, E.; von Heijne, G. *Protein Sci.* **1998**, *7*, 1029.
- (2) Sanders, C. R.; Myers, J. K. *Annu. Rev. Biophys. Biomol. Struct.* **2004**, *33*, 25.
- (3) White, S. *Membrane Proteins of Known 3D Structure*; <http://blanco.biomol.uci.edu/mpstruc/listAll/list> (January 16, 2012).
- (4) Warschawski, D. E. *Membrane Proteins of Known Structure Determined by NMR*; <http://www.drorlist.com/nmr.html> (January 16, 2012).
- (5) Opella, S. J.; Waugh, J. S. *J. Chem. Phys.* **1977**, *66*, 4919.
- (6) Schaefer, J.; Stejskal, E. O. *J. Am. Chem. Soc.* **1976**, *98*, 1031.
- (7) Cross, T. A.; Opella, S. J. *J. Am. Chem. Soc.* **1983**, *105*, 306.
- (8) Ketchum, R. R.; Hu, W.; Cross, T. A. *Science* **1993**, *261*, 1457.
- (9) Opella, S. J.; Marassi, F. M.; Gesell, J. J.; Valente, A. P.; Kim, Y.; Oblatt-Montal, M.; Montal, M. *Nat. Struct. Biol.* **1999**, *6*, 374.
- (10) Marassi, F. M.; Opella, S. J. *Protein Sci.* **2003**, *12*, 403.
- (11) Park, S. H.; Mrse, A. A.; Nevzorov, A. A.; Mesleh, M. F.; Oblatt-Montal, M.; Montal, M.; Opella, S. J. *J. Mol. Biol.* **2003**, *333*, 409.
- (12) De Angelis, A. A.; Howell, S. C.; Nevzorov, A. A.; Opella, S. J. *J. Am. Chem. Soc.* **2006**, *128*, 12256.
- (13) Sharma, M.; Yi, M.; Dong, H.; Qin, H.; Peterson, E.; Busath, D. D.; Zhou, H. X.; Cross, T. A. *Science* **2010**, *330*, 509.
- (14) Verardi, R.; Shi, L.; Traaseth, N. J.; Walsh, N.; Veglia, G. *Proc. Natl. Acad. Sci. U.S.A.* **2011**, *108*, 9101.
- (15) Nishimura, K.; Kim, S.; Zhang, L.; Cross, T. A. *Biochemistry* **2002**, *41*, 13170.
- (16) Cady, S. D.; Schmidt-Rohr, K.; Wang, J.; Soto, C. S.; Degrado, W. F.; Hong, M. *Nature* **2010**, *463*, 689.
- (17) Park, S. H.; Marassi, F. M.; Black, D.; Opella, S. J. *Biophys. J.* **2010**, *99*, 1465.
- (18) Sanders, C. R.; Hare, B.; Howard, K. P.; Prestegard, J. H. *Prog. NMR Spectrosc.* **1994**, *26*, 421.
- (19) Nicholson, L. K.; Moll, F.; Mixon, T. E.; LoGrasso, P. V.; Lay, J. C.; Cross, T. A. *Biochemistry* **1987**, *26*, 6621.
- (20) Bechinger, B.; Kim, Y.; Chirlian, L. E.; Gesell, J.; Neumann, J. M.; Montal, M.; Tomich, J.; Zasloff, M.; Opella, S. J. *J. Biomol. NMR* **1991**, *1*, 167.
- (21) De Angelis, A. A.; Nevzorov, A. A.; Park, S. H.; Howell, S. C.; Mrse, A. A.; Opella, S. J. *J. Am. Chem. Soc.* **2004**, *126*, 15340.
- (22) Casagrande, F.; Maier, K.; Kiefer, H.; Opella, S. J.; Park, S. H. In *Production of Membrane Proteins: Strategies for Expression and Isolation*; Robinson, A., Ed.; Wiley-VCH: New York, 2011.
- (23) Sinha, N.; Filipp, F. V.; Jaraim, L.; Park, S. H.; Bradley, J.; Opella, S. J. *Magn. Reson. Chem.* **2007**, *45*, S107.

- (24) Filipp, F. V.; Sinha, N.; Jairam, L.; Bradley, J.; Opella, S. J. *J. Magn. Reson.* **2009**, *201*, 121.
- (25) Wu, C. H.; Opella, S. J. *J. Magn. Reson.* **2008**, *190*, 165.
- (26) Lin, E. C.; Wu, C. H.; Yang, Y.; Grant, C. V.; Opella, S. J. *J. Magn. Reson.* **2010**, *206*, 105.
- (27) Wu, C. H.; Das, B. B.; Opella, S. J. *J. Magn. Reson.* **2010**, *202*, 127.
- (28) Lin, E. C.; Opella, S. J. *J. Magn. Reson.* **2011**, *211*, 37.
- (29) Cross, T. A.; DiVerdi, J. A.; Opella, S. J. *J. Am. Chem. Soc.* **1982**, *104*, 1759.
- (30) Sinha, N.; Grant, C. V.; Park, S. H.; Brown, J. M.; Opella, S. J. *J. Magn. Reson.* **2007**, *186*, 51.
- (31) Tycko, R. *Annu. Rev. Phys. Chem.* **2011**, *62*, 279.
- (32) Todokoro, Y.; Kobayashi, M.; Sato, T.; Kawakami, T.; Yumen, I.; Aimoto, S.; Fujiwara, T.; Akutsu, H. *J. Biomol. NMR* **2010**, *48*, 1.
- (33) Etzkorn, M.; Martell, S.; Andronesi, O. C.; Seidel, K.; Engelhard, M.; Baldus, M. *Angew. Chem., Int. Ed.* **2007**, *46*, 459.
- (34) Andreas, L. B.; Eddy, M. T.; Pielak, R. M.; Chou, J.; Griffin, R. G. *J. Am. Chem. Soc.* **2010**, *132*, 10958.
- (35) Cady, S. D.; Mishanina, T. V.; Hong, M. J. *Mol. Biol.* **2009**, *385*, 1127.
- (36) Shi, L.; Ahmed, M. A.; Zhang, W.; Whited, G.; Brown, L. S.; Ladizhansky, V. *J. Mol. Biol.* **2009**, *386*, 1078.
- (37) Su, Y.; Waring, A. J.; Ruchala, P.; Hong, M. *Biochemistry* **2011**, *50*, 2072.
- (38) Varga, K.; Tian, L.; McDermott, A. E. *Biochim. Biophys. Acta* **2007**, *1774*, 1604.
- (39) Huang, L.; McDermott, A. E. *Biochim. Biophys. Acta* **2008**, *1777*, 1098.
- (40) Li, Y.; Berthold, D. A.; Gennis, R. B.; Rienstra, C. M. *Protein Sci.* **2008**, *17*, 199.
- (41) Kijac, A. Z.; Li, Y.; Sligar, S. G.; Rienstra, C. M. *Biochemistry* **2007**, *46*, 13696.
- (42) Hiller, M.; Krabben, L.; Vinothkumar, K. R.; Castellani, F.; van Rossum, B. J.; Kuhlbrandt, W.; Oschkinat, H. *ChemBioChem* **2005**, *6*, 1679.
- (43) Schneider, R.; Etzkorn, M.; Giller, K.; Daebel, V.; Eisfeld, J.; Zweckstetter, M.; Griesinger, C.; Becker, S.; Lange, A. *Angew. Chem., Int. Ed.* **2010**, *49*, 1882.
- (44) Bauer, A. J.; Gieschler, S.; Lemberg, K. M.; McDermott, A. E.; Stockwell, B. R. *Biochemistry* **2011**, *50*, 3408.
- (45) Gullion, T.; Schaefer, J. *J. Magn. Reson. (1969-1992)* **1989**, *81*, 196.
- (46) Jaroniec, C. P.; MacPhee, C. E.; Bajaj, V. S.; McMahon, M. T.; Dobson, C. M.; Griffin, R. G. *Proc. Natl. Acad. Sci. U.S.A.* **2004**, *101*, 711.
- (47) Opella, S. J.; Frey, M. H.; Cross, T. A. *J. Am. Chem. Soc.* **1979**, *101*, 5856.
- (48) Edidin, M. *Annu. Rev. Biophys. Bioeng.* **1974**, *3*, 179.
- (49) Cherry, R. J. *FEBS Lett.* **1975**, *55*, 1.
- (50) McLaughlin, A. C.; Cullis, P. R.; Hemminga, M. A.; Hoult, D. I.; Radda, G. K.; Ritchie, G. A.; Seeley, P. J.; Richards, R. E. *FEBS Lett.* **1975**, *57*, 213.
- (51) Lewis, B. A.; Harbison, G. S.; Herzfeld, J.; Griffin, R. G. *Biochemistry* **1985**, *24*, 4671.
- (52) Park, S. H.; Mrse, A. A.; Nevzorov, A. A.; De Angelis, A. A.; Opella, S. J. *J. Magn. Reson.* **2006**, *178*, 162.
- (53) Park, S. H.; Casagrande, F.; Das, B. B.; Albrecht, L.; Chu, M.; Opella, S. J. *Biochemistry* **2011**, *50*, 2371.
- (54) Mahalakshmi, R.; Franzin, C. M.; Choi, J.; Marassi, F. M. *Biochim. Biophys. Acta* **2007**, *1768*, 3216.
- (55) Kovacs, F. A.; Cross, T. A. *Biophys. J.* **1997**, *73*, 2511.
- (56) De Angelis, A. A.; Jones, D. H.; Grant, C. V.; Park, S. H.; Mesleh, M. F.; Opella, S. J. *Methods Enzymol.* **2005**, *394*, 350.
- (57) Cady, S. D.; Goodman, C.; Tatko, C. D.; DeGrado, W. F.; Hong, M. *J. Am. Chem. Soc.* **2007**, *129*, 5719.
- (58) Park, S. H.; Das, B. B.; De Angelis, A. A.; Scrima, M.; Opella, S. J. *J. Phys. Chem. B* **2010**, *114*, 13995.
- (59) Chan, J. C. C.; Tycko, R. *J. Chem. Phys.* **2003**, *118*, 8378.
- (60) Wylie, B. J.; Franks, W. T.; Rienstra, C. M. *J. Phys. Chem. B* **2006**, *110*, 10926.
- (61) Mou, Y.; Chen, P. H.; Lee, H. W.; Chan, J. C. *J. Magn. Reson.* **2007**, *187*, 352.
- (62) Marassi, F. M.; Das, B. B.; Lu, G. J.; Nothnagel, H. J.; Park, S. H.; Son, W. S.; Tian, Y.; Opella, S. J. *Methods* **2012**, *10.1016/j.ymeth.2011.09.009*.
- (63) Barkay, T.; Miller, S. M.; Summers, A. O. *FEMS Microbiol. Rev.* **2003**, *27*, 355.
- (64) Howell, S. C.; Mesleh, M. F.; Opella, S. J. *Biochemistry* **2005**, *44*, 5196.
- (65) Mao, L.; Inoue, K.; Tao, Y.; Montelione, G. T.; McDermott, A. E.; Inouye, M. *J. Biomol. NMR* **2011**, *49*, 131.
- (66) Thankur, R. S.; Kurur, N. D.; Madhu, P. K. *Chem. Phys. Lett.* **2006**, *426*, 459.
- (67) Shaka, A. J.; Keeler, J. M.; Freeman, R. *J. Magn. Reson. (1969-1992)* **1983**, *53*, 313.
- (68) Pines, A.; Gibby, M. G.; Waugh, J. S. *J. Chem. Phys.* **1972**, *56*, 1776.
- (69) Baldus, M.; Petkova, A.; Herzfeld, J.; Griffin, R. *Mol. Phys.* **1998**, *95*, 1197.
- (70) Lewandowski, J. R.; De Paepe, G.; Griffin, R. G. *J. Am. Chem. Soc.* **2007**, *129*, 728.
- (71) Bloembergen, N. *Phys. Chem. Chem. Phys.: PCCP* **1949**, *15*, 386.
- (72) Szeverenyi, N. M.; Sullivan, M. J.; Maciel, G. E. *J. Magn. Reson. (1969-1992)* **1982**, *47*, 462.
- (73) Frey, M. H.; Opella, S. J. *J. Am. Chem. Soc.* **1984**, *106*, 4942.
- (74) Kakegoshi, K.; Nakamura, S.; Terao, T. *Chem. Phys. Lett.* **2001**, *344*, 631.
- (75) Wylie, B. J.; Rienstra, C. M. *J. Chem. Phys.* **2008**, *128*, 052207.
- (76) Zhao, X.; Eden, M.; Levitt, M. H. *Chem. Phys. Lett.* **2001**, *342*, 353.
- (77) Petkova, A. T.; Baldus, M.; Belenky, M.; Hong, M.; Griffin, R. G.; Herzfeld, J. *J. Magn. Reson.* **2003**, *160*, 1.
- (78) States, D. J.; Haberkorn, R. A.; Ruben, D. J. *J. Magn. Reson. (1969-1992)* **1982**, *48*, 286.
- (79) Das, R.; Baker, D. *Annu. Rev. Biochem.* **2008**, *77*, 363.
- (80) Yarov-Yarovoy, V.; Schonbrun, J.; Baker, D. *Proteins* **2006**, *62*, 1010.
- (81) Schwieters, C. D.; Kuszewski, J. J.; Tjandra, N.; Clore, G. M. *J. Magn. Reson.* **2003**, *160*, 65.
- (82) DeLano, W. L. PyMOL. www.pymol.org (January 16, 2012).
- (83) Baker, D. *Robetta: Full-chain Protein Structure Prediction Server* <http://robetta.bakerlab.org/> (January 16, 2012).
- (84) Schwieters, C. D.; Clore, G. M. *J. Magn. Reson.* **2001**, *152*, 288.
- (85) Kuszewski, J.; Gronenborn, A. M.; Clore, G. M. *J. Magn. Reson.* **1997**, *125*, 171.
- (86) Nilges, M.; Clore, G. M.; Gronenborn, A. M. *FEBS Lett.* **1988**, *239*, 129.
- (87) Oas, T. G.; Hartzell, C. J.; Dahlquist, W.; Drobny, G. P. *J. Am. Chem. Soc.* **1987**, *109*, 5962.
- (88) Wilson, J. R.; Leang, C.; Morby, A. P.; Hobman, J. L.; Brown, N. L. *FEBS Lett.* **2000**, *472*, 78.
- (89) Herzfeld, J.; Berger, A. E. *J. Chem. Phys.* **1980**, *73*, 6021.
- (90) Markley, J. L. *Biological Magnetic Resonance Data Bank*; www.bmrwisc.edu/ (January 16, 2012).
- (91) Mesleh, M. F.; Veglia, G.; DeSilva, T. M.; Marassi, F. M.; Opella, S. J. *J. Am. Chem. Soc.* **2002**, *124*, 4206.
- (92) Opella, S. J.; Marassi, F. M. *Chem. Rev.* **2004**, *104*, 3587.
- (93) Cross, T. A.; Sharma, M.; Yi, M.; Zhou, H. X. *Trends Biochem. Sci.* **2011**, *36*, 117.